JOURNAL OF MODERN OPTICS, 2017
VOL. 64, NOS. 10–11, 987–994
https://doi.org/10.1080/09500340.2016.1265678

Taylor & Francis
Taylor & Francis Group

Spin-polarized photoelectrons produced by strong-field ionization of randomly aligned nitric oxide

Kunlong Liu and Ingo Barth

Max Planck Institute of Microstructure Physics, Halle (Saale), Germany

ABSTRACT

We investigate the effect of the molecular alignment of nitric oxide (NO) on nonadiabatic tunnel ionization of degenerate valence $\pi_\pm$ orbitals in strong circularly polarized laser fields and on spin polarization of photoelectrons. Our numerical study shows that not only for the alignment parallel to the laser propagation axis [Liu, K.; Barth, I. *Phys. Rev. A* **2016**, *94*, 043402] but also for arbitrary alignment angles except for perpendicular alignment, the counter-rotating molecular orbital with respect to the circular polarization of the laser field projected on the plane perpendicular to the molecular axis is ionized more easily. Due to the nonadiabatic effect and the nodal structure of the valence $2\pi_\pm$ orbitals of NO, the ionization maxima for the $2\pi_-$ and $2\pi_+$ orbitals in right circularly polarized laser fields are obtained for the molecular orientations at the polar angles of around 60° and 120°, respectively. Considering the spin-orbital entanglement in the doubly degenerate electronic ground state of NO, the spin-polarization of photoelectrons is high for parallel alignment, decreases upon increasing the polar angle and vanishes for perpendicular alignment. Averaging over all alignment angles, non-zero spin-polarization of photoelectrons for randomly aligned NO is preserved.

ARTICLE HISTORY
Received 11 October 2016
Accepted 21 November 2016

KEYWORDS
Spin polarization; tunnel ionization; circularly polarized laser field; molecular alignment

1. Introduction

In attosecond physics, strong-field ionization of atoms and molecules has been studied extensively for decades (*1*). The studies exploring electronic dynamics after ionization have stimulated many interesting topics such as high harmonic generation (*2*–*5*), tomographic imaging (*6*), attosecond angular streaking (*7*, *8*), laser-induced electron diffraction (*9*–*12*), photoelectron holography (*13*, *14*), and electron-nuclear energy sharing (*15*–*17*). Currently, there is broad interest to play with the electron spin in the realm of attoscience to reveal the spin-resolved dynamics in atoms and molecules using ultrashort spin-polarized electron beams. To achieve this goal, one has to think about production of perfectly spin-polarized electrons on the attosecond time scale. For example, it has been shown theoretically that a bichromatic circularly polarized laser field can produce spin-polarized electrons (*18*), whereas the production of spin-polarized photoelectrons by ionization of noble gas in strong monochromatic circularly polarized laser fields has been very recently performed in the experiment (*19*). This effect is based on the theory of nonadiabatic ionization of degenerate valence p atomic orbitals in strong circularly polarized laser fields (*20*, *21*). This theory has also been verified by numerical calculations for broad range of laser parameters (*22*, *23*) and shows that in general the initial counter-rotating electron with respect to the circular polarization of the laser field is removed more easily, i.e. for right circular polarization the ionization of the p_- orbital is preferred over the ionization of the p_+ orbital. This theoretical prediction has been partially confirmed by the sequential double ionization experiment (*24*, *25*). Finally, due to the existence of spin-orbit couplings in ionic states of noble gas that causes spin-orbit entanglement, it has been shown in both theory (*26*) and experiment (*19*) that the strong-field ionization of noble gas by circularly polarized laser pulses can produce spin-polarized photoelectrons.

Very recently, we have developed the theory of nonadiabatic ionization of the pre-aligned linear nitric oxide (NO) molecule possessing degenerate valence $\pi_\pm$ orbitals in strong circularly polarized laser fields (*27*). By numerically solving the three-dimensional time-dependent Schrödinger equation (3D-TDSE) for a single valence electron of NO and for different laser parameters, we have verified our theory successfully, also with consideration of laser-dressed orbitals for slowly rotating and very strong circularly polarized laser fields (*27*). Similar to atoms, we have predicted that in general the counter-rotating molecular π orbital is ionized more

CONTACT Ingo Barth barth@mpi-halle.mpg.de

easily, i.e. the ionization of the π_- orbital of the pre-aligned linear molecule in right circularly polarized laser fields is preferred. Since the doubly degenerate electronic ground state $|X\,^2\Pi_{1/2}\rangle$ of NO has two possible electron configurations $\pi_+^{\downarrow}$ and $\pi_-^{\uparrow}$, the preferred ionization of the counter-rotating molecular orbital leads to the production of photoelectrons with controllable spin polarization up to 100% (*27*).

In this work, we perform numerical simulations for nonadiabatic tunnel ionization of degenerate valence $2\pi_\pm$ orbitals of NO for different molecular alignments with respect to the strong circularly polarized laser field. The details of numerical calculations are described in Section 2. To obtain the analytical expression for the spin polarization of photoelectrons for arbitrary alignment angles, we develop the theory of the spin polarization in Section 3. The results of our calculations are presented and discussed in Section 4 and the conclusions of this work are summarized in Section 5.

2. Numerical calculation

We consider an arbitrarily aligned NO molecule in the electronic ground state $|X\,^2\Pi_\pm\rangle$ ionized by a three-cycle strong right circularly polarized laser pulse, see Figure 1. Since the $|X\,^2\Pi_\pm\rangle$ state is doubly degenerate and contains only one valence electron in the degenerate molecular $2\pi_\pm$ orbital, we solve the length-gauge 3D-TDSE within the single active electron (SAE) approximation for different alignment angles of NO, here for polar angles $\alpha = 0°, 10°, 20°, \ldots, 170°$ and azimuthal angles $\beta = 0°, 90°, 180°, 270°$. For the detailed study of the weak β-dependence due to the asymmetry of the few-cycle laser pulse, we also perform numerical simulations for $\alpha = 10°$ and $\beta = 0°, 30°, 60°, \ldots, 330°$. We note that $\alpha = 0°$ and $\alpha = 90°$ correspond to the parallel and perpendicular alignments of NO with respect to the laser propagation axis, respectively. In particular, we solve the 3D-TDSE for two possible initial electronic states $|X\,^2\Pi_-\rangle$ and $|X\,^2\Pi_+\rangle$, corresponding to the initial $2\pi_-$ and $2\pi_+$ orbitals in the SAE approximation, respectively, and for the laser wavelength $\lambda = 800$ nm and the electric field amplitude $\mathcal{E} = 0.05$ a.u., corresponding to the laser intensity 1.76×10^{14} W/cm^2. We define the initial $2\pi_-$ and $2\pi_+$ orbitals in the molecular frame so that the initial electron rotates clockwise and counterclockwise around the molecular z'-axis, respectively, cf. Figure 1. Thus for $\alpha = 0°$, the $2\pi_-$ orbital with respect to the right circular polarization of the laser field is counter-rotating, while for $\alpha = 180°$, the same $2\pi_-$ orbital is co-rotating. In general, for alignment angles $\alpha = [0°, 90°)$ and $\alpha = (90°, 180°]$, the $2\pi_-$ orbital is counter-rotating and co-rotating with

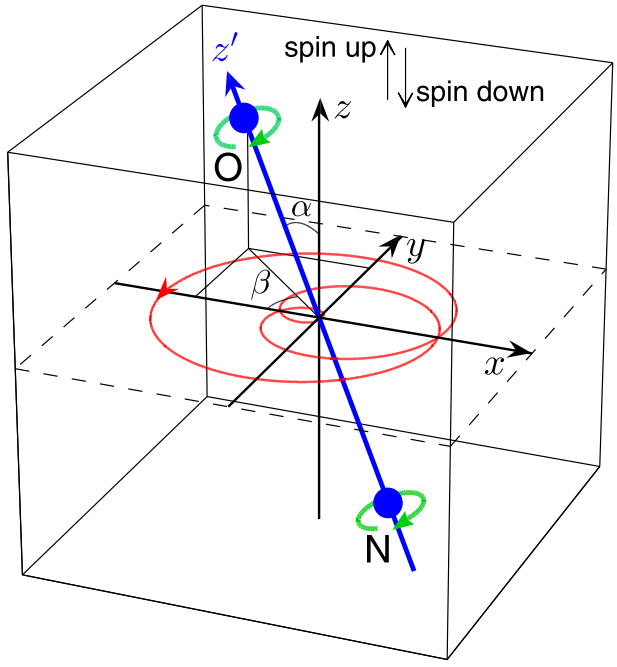

Figure 1. Schematic illustration of the ionization of the NO molecule with its molecular axis (blue thick line) in a three-cycle strong right circularly polarized laser pulse (red thin curve on the x/y-plane with its arrow indicating anticlockwise rotation of the electric field vector) propagating along the z-axis of the laboratory xyz-frame. The molecular alignment of NO is determined by the polar angle α and the azimuthal angle β, where the O atom lies on the positive molecular z'-axis. Two green thick curves around the NO molecule indicate the counter-rotating valence $2\pi_-$ orbital. The positive and negative z-axes of the laboratory frame are chosen as reference axes for spin-up and spin-down polarizations, respectively.

respect to the right circular polarization of the laser field projected on the plane perpendicular to the molecular axis, respectively, see also Figure 2(b). For the $2\pi_+$ orbital, these counter- and co-rotating properties are reversed. The solutions of the 3D-TDSE are the single electron wave functions $\psi_-(\alpha, \beta, \mathbf{r}, t)$ and $\psi_+(\alpha, \beta, \mathbf{r}, t)$ for the initial molecular $2\pi_-$ and $2\pi_+$ orbitals, respectively. Using the masking function to absorb the outgoing wave packet, we calculate the corresponding time-independent ionization yields depending on the alignment angles at the end of propagation time sufficiently long after the end of the laser pulse, i.e.

$$Y_\pm(\alpha, \beta) = 1 - \lim_{t\to\infty} \langle \psi_\pm(\alpha, \beta, t) | \psi_\pm(\alpha, \beta, t) \rangle_V, \quad (1)$$

where the integration is over the finite volume V. The details of the numerical 3D-TDSE calculations for the valence electron of NO on a Cartesian 3D grid are found in Ref. (*27*).

3. Spin polarization

In the presence of spin-orbit coupling, the electronic ground state $|X\,^2\Pi_\pm\rangle$ of the NO molecule is split into two doubly degenerate states $|X\,^2\Pi_{1/2}\rangle$ and $|X\,^2\Pi_{3/2}\rangle$, separated by about $120\,\mathrm{cm}^{-1}$ (0.015 eV). In this work, we only consider the energetically lowest state $|X\,^2\Pi_{1/2}\rangle$ containing two possible valence electron configurations $2\pi_-^\uparrow$ ($m_j = -1/2$) and $2\pi_+^\downarrow$ ($m_j = 1/2$) in the molecular frame, i.e. the spin-up and spin-down electrons of the valence $2\pi_\pm$ orbitals are directed to the positive and negative molecular z'-axes described by spin wave functions $\chi_{z'}^\uparrow$ and $\chi_{z'}^\downarrow$, respectively. Since the effect of the non-relativistic laser field with intensity well below $10^{16}\,\mathrm{W/cm^2}$ on the electron spin is negligible, we assume that the spin of the electron does not change during interaction with the laser pulse; for spin-flip of the photoelectron in relativistic laser fields see Refs. (*28*, *29*). Then, starting from the electronic ground state $|X\,^2\Pi_{1/2}\rangle$ of arbitrarily aligned NO, the time-dependent single electron wave functions including spin in the molecular frame are given by

$$\Psi_-(\alpha,\beta,\mathbf{r},t) = \psi_-(\alpha,\beta,\mathbf{r},t)\chi_{z'}^\uparrow, \tag{2}$$

$$\Psi_+(\alpha,\beta,\mathbf{r},t) = \psi_+(\alpha,\beta,\mathbf{r},t)\chi_{z'}^\downarrow \tag{3}$$

for the electron starting from the $2\pi_-^\uparrow$ and $2\pi_+^\downarrow$ spin-orbital, respectively.

To obtain the expressions for the probabilities of detecting the spin-up and spin-down photoelectrons in the laboratory frame, we start to deal with the Cartesian components of the spin operator in the molecular frame given by

$$\hat{S}_{x'} = \frac{\hbar}{2}\hat{\sigma}_{x'},\ \hat{S}_{y'} = \frac{\hbar}{2}\hat{\sigma}_{y'},\ \hat{S}_{z'} = \frac{\hbar}{2}\hat{\sigma}_{z'}, \tag{4}$$

with the corresponding Pauli matrices for the electron

$$\hat{\sigma}_{x'} = \begin{pmatrix} 0 & 1 \\ 1 & 0 \end{pmatrix},\quad \hat{\sigma}_{y'} = \begin{pmatrix} 0 & -i \\ i & 0 \end{pmatrix},$$
$$\hat{\sigma}_{z'} = \begin{pmatrix} 1 & 0 \\ 0 & -1 \end{pmatrix}. \tag{5}$$

For the arbitrary unit vector $\vec{v} = (v_{x'}, v_{y'}, v_{z'})$ with its Cartesian components $v_{x'}, v_{y'}, v_{z'}$ in the molecular coordinate system, the electron spin operator with respect to the direction of this vector is simply defined as:

$$\begin{aligned}\hat{S}_v &= \frac{\hbar}{2}\hat{\sigma}_v = v_{x'}\hat{S}_{x'} + v_{y'}\hat{S}_{y'} + v_{z'}\hat{S}_{z'} \\ &= \frac{\hbar}{2}(v_{x'}\hat{\sigma}_{x'} + v_{y'}\hat{\sigma}_{y'} + v_{z'}\hat{\sigma}_{z'}).\end{aligned} \tag{6}$$

The normalized eigenvectors of $\hat{\sigma}_v$ in Equation (6) can be derived straightforwardly and we obtain

$$\chi_v^\uparrow = \begin{cases} \begin{pmatrix} 0 \\ 1 \end{pmatrix} & \text{for } v_{z'} = -1, \\ (2+2v_{z'})^{-1/2}\begin{pmatrix} 1+v_{z'} \\ v_{x'}+iv_{y'} \end{pmatrix} & \text{for } v_{z'} \neq -1, \end{cases} \tag{7}$$

$$\chi_v^\downarrow = \begin{cases} \begin{pmatrix} 0 \\ 1 \end{pmatrix} & \text{for } v_{z'} = 1, \\ (2-2v_{z'})^{-1/2}\begin{pmatrix} -1+v_{z'} \\ v_{x'}+iv_{y'} \end{pmatrix} & \text{for } v_{z'} \neq 1 \end{cases} \tag{8}$$

with corresponding eigenvalues 1 and -1, respectively. Thus, the spin eigenvectors $\chi_v^\uparrow$ and $\chi_v^\downarrow$ correspond to spin-up and spin-down electrons with respect to the direction of the given vector $\vec{v}$, respectively. In particular, with respect to the direction of the molecular z'-axis, i.e. $v_{x'} = v_{y'} = 0, v_{z'} = 1$, we obtain from Equations (7) and (8) the well-known spin wave functions as

$$\chi_{z'}^\uparrow = \begin{pmatrix} 1 \\ 0 \end{pmatrix}, \tag{9}$$

$$\chi_{z'}^\downarrow = \begin{pmatrix} 0 \\ 1 \end{pmatrix}. \tag{10}$$

If the direction of the unit vector $\vec{v}$ in the molecular frame is equal to the direction of the positive z-axis of the laboratory frame, then we obtain from Equations (7) and (8) the spin wave functions with respect to the z-axis of the laboratory frame as

$$\chi_z^\uparrow = (2+2\cos\alpha)^{-1/2}\begin{pmatrix} 1+\cos\alpha \\ -e^{-i\beta}\sin\alpha \end{pmatrix}, \tag{11}$$

$$\chi_z^\downarrow = (2-2\cos\alpha)^{-1/2}\begin{pmatrix} -1+\cos\alpha \\ -e^{-i\beta}\sin\alpha \end{pmatrix}, \tag{12}$$

where $v_{x'} = -\sin\alpha\cos\beta$, $v_{y'} = \sin\alpha\sin\beta$, and $v_{z'} = \cos\alpha$ (cf. Figure 1) were used. Using the spectral theorem, we get for an arbitrary vector $\vec{v}$

$$\chi_{z'}^\uparrow = \langle\chi_{z'}^\uparrow|\chi_v^\uparrow\rangle\chi_v^\uparrow + \langle\chi_{z'}^\uparrow|\chi_v^\downarrow\rangle\chi_v^\downarrow \tag{13}$$

$$\chi_{z'}^\downarrow = \langle\chi_{z'}^\downarrow|\chi_v^\uparrow\rangle\chi_v^\uparrow + \langle\chi_{z'}^\downarrow|\chi_v^\downarrow\rangle\chi_v^\downarrow, \tag{14}$$

and in particular for the vector $\vec{\nu}$ directed to the positive z-axis of the laboratory frame

$$\chi_{z'}^{\uparrow} = \sqrt{\frac{1+\cos\alpha}{2}}\,\chi_z^{\uparrow} - \sqrt{\frac{1-\cos\alpha}{2}}\,\chi_z^{\downarrow} \tag{15}$$

$$\chi_{z'}^{\downarrow} = -e^{-i\beta}\sqrt{\frac{1-\cos\alpha}{2}}\,\chi_z^{\uparrow} - e^{-i\beta}\sqrt{\frac{1+\cos\alpha}{2}}\,\chi_z^{\downarrow}. \tag{16}$$

The electron wave functions including spin (Equations (2) and (3)) are then split into spin-up and spin-down electron wave functions with respect to the reference z-axis of the laboratory frame, i.e.

$$\Psi_-(\alpha,\beta,\mathbf{r},t) = \Psi_-^{\uparrow}(\alpha,\beta,\mathbf{r},t) + \Psi_-^{\downarrow}(\alpha,\beta,\mathbf{r},t), \tag{17}$$

$$\Psi_+(\alpha,\beta,\mathbf{r},t) = \Psi_+^{\uparrow}(\alpha,\beta,\mathbf{r},t) + \Psi_+^{\downarrow}(\alpha,\beta,\mathbf{r},t), \tag{18}$$

where

$$\Psi_-^{\uparrow}(\alpha,\beta,\mathbf{r},t) = \sqrt{\frac{1+\cos\alpha}{2}}\,\psi_-(\alpha,\beta,\mathbf{r},t)\chi_z^{\uparrow}, \tag{19}$$

$$\Psi_-^{\downarrow}(\alpha,\beta,\mathbf{r},t) = -\sqrt{\frac{1-\cos\alpha}{2}}\,\psi_-(\alpha,\beta,\mathbf{r},t)\chi_z^{\downarrow} \tag{20}$$

are the spin-up and spin-down (now always referred to the z-axis of the laboratory frame) electron wave functions starting from the $2\pi_-$ orbital and

$$\Psi_+^{\uparrow}(\alpha,\beta,\mathbf{r},t) = -e^{-i\beta}\sqrt{\frac{1-\cos\alpha}{2}}\,\psi_+(\alpha,\beta,\mathbf{r},t)\chi_z^{\uparrow}, \tag{21}$$

$$\Psi_+^{\downarrow}(\alpha,\beta,\mathbf{r},t) = -e^{-i\beta}\sqrt{\frac{1+\cos\alpha}{2}}\,\psi_+(\alpha,\beta,\mathbf{r},t)\chi_z^{\downarrow} \tag{22}$$

are the spin-up and spin-down electron wave functions starting from the $2\pi_+$ orbital. Similarly, the expressions for other reference axes for the electron spin could also be derived, but we expect the highest spin polarization for the reference z-axis of the laboratory frame. So, as from now, we focus on the laboratory z-axis as the reference axis for the electron spin.

The probabilities of detecting the spin-up and spin-down photoelectrons in the laboratory frame sufficiently long after the end of the laser pulse are

$$Y_{\pm}^{\uparrow}(\alpha,\beta) = \lim_{t\to\infty}\Big(\langle\Psi_{\pm}^{\uparrow}(\alpha,\beta,t)|\Psi_{\pm}^{\uparrow}(\alpha,\beta,t)\rangle - \langle\Psi_{\pm}^{\uparrow}(\alpha,\beta,t)|\Psi_{\pm}^{\uparrow}(\alpha,\beta,t)\rangle_V\Big), \tag{23}$$

$$Y_{\pm}^{\downarrow}(\alpha,\beta) = \lim_{t\to\infty}\Big(\langle\Psi_{\pm}^{\downarrow}(\alpha,\beta,t)|\Psi_{\pm}^{\downarrow}(\alpha,\beta,t)\rangle - \langle\Psi_{\pm}^{\downarrow}(\alpha,\beta,t)|\Psi_{\pm}^{\downarrow}(\alpha,\beta,t)\rangle_V\Big), \tag{24}$$

where the integration of the second term is over the finite volume V. Using Equations (1), (19)–(22), we obtain the alignment-dependent spin-up and spin-down ionization yields

$$Y_-^{\uparrow}(\alpha,\beta) = \frac{1+\cos\alpha}{2}\,Y_-(\alpha,\beta), \tag{25}$$

$$Y_-^{\downarrow}(\alpha,\beta) = \frac{1-\cos\alpha}{2}\,Y_-(\alpha,\beta), \tag{26}$$

for the initial $2\pi_-$ orbital and

$$Y_+^{\uparrow}(\alpha,\beta) = \frac{1-\cos\alpha}{2}\,Y_+(\alpha,\beta), \tag{27}$$

$$Y_+^{\downarrow}(\alpha,\beta) = \frac{1+\cos\alpha}{2}\,Y_+(\alpha,\beta), \tag{28}$$

for the initial $2\pi_+$ orbital. The spin-independent ionization yields $Y_{\pm}(\alpha,\beta) = Y_{\pm}^{\uparrow}(\alpha,\beta) + Y_{\pm}^{\downarrow}(\alpha,\beta)$ (Equation (1)) are obtained from numerical 3D-TDSE calculations. Assuming that the ensemble of NO molecules contains equal amounts of valence $2\pi_-$ and $2\pi_+$ electrons, we are able to calculate alignment-dependent total ionization yields of spin-up and spin-down photoelectrons according to

$$Y^{\uparrow}(\alpha,\beta) = Y_-^{\uparrow}(\alpha,\beta) + Y_+^{\uparrow}(\alpha,\beta), \tag{29}$$

$$Y^{\downarrow}(\alpha,\beta) = Y_-^{\downarrow}(\alpha,\beta) + Y_+^{\downarrow}(\alpha,\beta), \tag{30}$$

respectively. Furthermore, the total spin-independent ionization yield is defined as:

$$Y_{\text{total}}(\alpha,\beta) = Y^{\uparrow}(\alpha,\beta) + Y^{\downarrow}(\alpha,\beta) = Y_-(\alpha,\beta) + Y_+(\alpha,\beta). \tag{31}$$

Then, the spin polarization of photoelectrons as a function of alignment angles α and β is calculated as

$$\mathcal{P}(\alpha,\beta) = \frac{Y^{\uparrow}(\alpha,\beta) - Y^{\downarrow}(\alpha,\beta)}{Y_{\text{total}}(\alpha,\beta)}. \tag{32}$$

Averaging over all molecular alignments, we calculate the average total ionization yields of spin-up and spin-down

photoelectrons as

$$\overline{Y}^{\uparrow} = \frac{1}{4\pi}\int_0^{2\pi} \mathrm{d}\beta \int_0^{\pi} \mathrm{d}\alpha\, Y^{\uparrow}(\alpha,\beta)\sin\alpha, \tag{33}$$

$$\overline{Y}^{\downarrow} = \frac{1}{4\pi}\int_0^{2\pi} \mathrm{d}\beta \int_0^{\pi} \mathrm{d}\alpha\, Y^{\downarrow}(\alpha,\beta)\sin\alpha \tag{34}$$

and the corresponding average spin polarization of photoelectrons as

$$\overline{\mathcal{P}} = \frac{\overline{Y}^{\uparrow} - \overline{Y}^{\downarrow}}{\overline{Y}^{\uparrow} + \overline{Y}^{\downarrow}}. \tag{35}$$

4. Results and discussion

Numerical results of ionization yields and spin polarization of photoelectrons depending on the molecular alignment of NO are shown in Figures 2 and 3, where we only show the fitted curves in Figure 2 for better visibility. In particular, all results show strong dependence on the polar angle α, whereas the weak dependence on the azimuthal angle β is due to the asymmetry of the three-cycle circularly polarized laser pulse, cf. Figure 1. We note that the β-dependence vanishes for continuous wave (cw) circularly polarized laser fields. Figure 2 shows that the β-dependence of ionization yields (with larger values for $\beta = 0°$) is more visible than that of spin polarization, because the spin polarization (Equation (32)) is calculated as the relative difference of ionization yields of spin-up and spin-down photoelectrons. Furthermore, we emphasize that all numerical results for $\beta = 90°$ and $\beta = 270°$ are very similar but not identical, because the NO molecule is heteronuclear and its valence $2\pi_{\pm}$ orbitals consist of two slightly different π-phase shifted atomic $2p_{\pm}$ orbitals carrying electron ring currents about N and O nuclei; for generation of electron ring currents about the axis of pre-oriented heteronuclear linear molecules see Refs. (*30*, *31*).

Figure 2(a) shows the total ionization yield $Y_{\mathrm{total}}(\alpha,\beta)$ of photoelectrons (Equation (31)) for an initial ensemble of NO molecules containing equal amounts of $2\pi_+$ and $2\pi_-$ valence electrons. For circularly polarized laser pulses, the total ionization yield of photoelectrons from NO exhibits a plateau between $\alpha = 60°$ and $\alpha = 120°$ with maxima around $\alpha = 60°$–$70°$ as well as $\alpha = 110°$–$120°$. The results for linear polarization of the laser field would be different and we except that in this case the maxima would lie around $\alpha = 45°$ and $\alpha = 135°$ that would correspond to the experimental results of the momentum imaging of N^+ fragment ions produced by dissociative ionization from the electronic ground state of NO (*32*). Furthermore, the $2\pi_{\pm}$ orbital of NO is similar to the valence orbital of O_2 and there are experimental

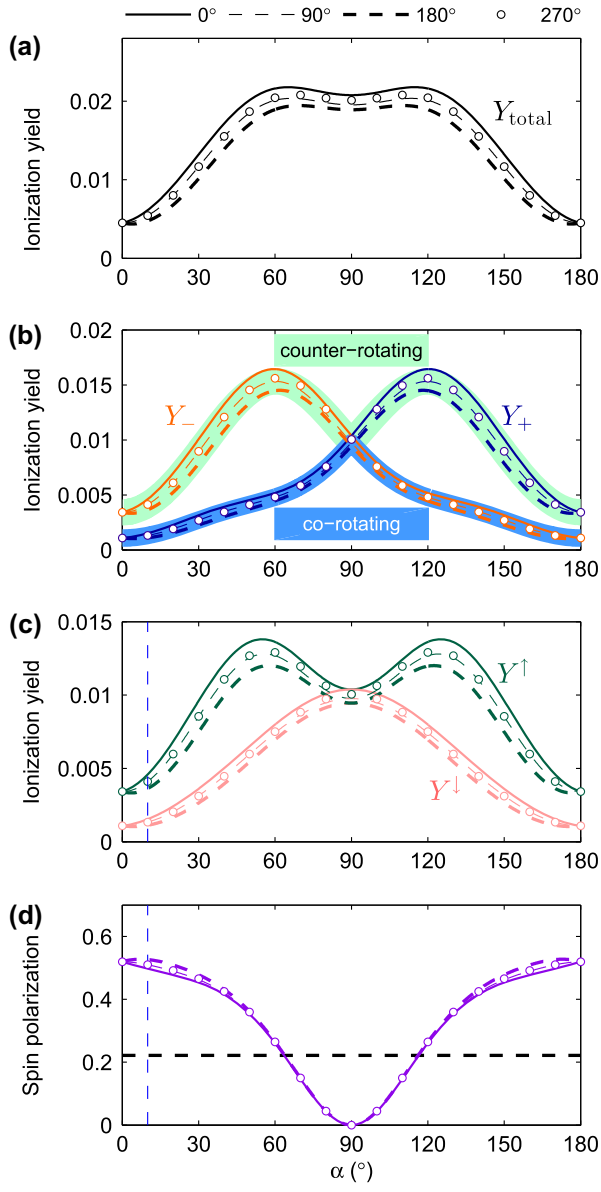

Figure 2. Ionization yields (a-c) and spin polarization (d) of photoelectrons ejected from the valence molecular $2\pi_{\pm}$ orbitals of NO by a strong right circularly polarized laser pulse depending on the molecular alignment, i.e. depending on the polar angle α for $\beta = 0°$ (solid), $\beta = 90°$ (thin dashed), $\beta = 180°$ (thick dashed), and $\beta = 270°$ (circles). (a) Total spin-independent ionization yield $Y_{\mathrm{total}}(\alpha,\beta)$ (black, Equation (31)). (b) Spin-independent ionization yields $Y_-(\alpha,\beta)$ (orange light) and $Y_+(\alpha,\beta)$ (blue dark) of photoelectrons starting from $2\pi_-$ and $2\pi_+$ orbitals, respectively (Equation (1)). The initial counter-rotating and co-rotating orbitals with respect to the circular polarization of the laser field projected on the plane perpendicular to the molecular axis are shown in (b) as green light and blue dark shades, respectively. (c) Total ionization yields of spin-up $Y^{\uparrow}(\alpha,\beta)$ (green dark, Equation (29)) and spin-down $Y^{\downarrow}(\alpha,\beta)$ (red light, Equation (30)) photoelectrons. (d) Spin polarization of photoelectrons $\mathcal{P}(\alpha,\beta)$ (violet, Equation (32)). The horizontal black dashed line in (d) shows the average spin polarization $\overline{\mathcal{P}} = 22.1\%$ (Equation (35)). The vertical blue dashed lines in (c) and (d) show the β-dependence of the ionization yields and spin polarization for $\alpha = 10°$ in Figure 3.

and numerical results of total ionization yields for O_2 and for linear polarization with maxima around $\alpha = 45°$ and $\alpha = 135°$, see Refs. (*33*, *34*). However, to best of our knowledge, there are no experimental results of alignment-dependent total ionization yields for NO or O_2 and for circular polarization. Therefore, we here only present our numerical results for circular polarization.

The total ionization yield $Y_{\text{total}}(\alpha, \beta)$ consists of the ionization yields $Y_-(\alpha, \beta)$ and $Y_+(\alpha, \beta)$ of photoelectrons (Equation (1)) ejected from the valence $2\pi_-$ and $2\pi_+$ orbitals of NO, respectively. These orbital-resolved ionization yields shown in Figure 2(b) are obtained by solving the 3D-TDSE numerically. As already explained in Section 2, the $2\pi_-$ orbital for $\alpha = [0°, 90°)$ and $\alpha = (90°, 180°]$ is counter-rotating and co-rotating with respect to the right circular polarization of the laser field projected on the plane perpendicular to the molecular axis, whereas these properties for the $2\pi_+$ orbital are reversed. The alignment-dependent ionization yields of counter- and co-rotating orbitals are clearly shown in Figure 2(b). In particular, the counter-rotating valance molecular orbital of NO with respect to the right circular polarization of the laser field is ionized more easily for all alignment angles except for $\alpha = 90°$. Apparently, the ionization yield of the photoelectron from the counter-rotating orbital of NO (probably also for O_2 due to the similar valence orbital) has the maxima at around $\alpha = 60°$ and $\alpha = 120°$, whereas for the co-rotating orbital there is no local maximum of the ionization yield except for $\alpha = 90°$. For perpendicular molecular alignment, the ionization yields of counter- and co-rotating orbitals are identical.

Figure 2(c) presents the total ionization yields of spin-up $Y^{\uparrow}(\alpha, \beta)$ and spin-down $Y^{\downarrow}(\alpha, \beta)$ photoelectrons, obtained from Equations (29) and (30), where the spin-up and spin-down electrons are referred to the positive and negative z-axes of the laboratory frame, respectively. It clearly shows that spin-up photoelectrons are dominant for all alignment angles except for perpendicular alignment. This dominance is related to the dominance of the photoelectrons ejected from counter-rotating orbitals, see Figure 2(c). The ionization yield of the spin-up photoelectron has the maximum at around $\alpha = 50°-60°$ and $\alpha = 120°$–$130°$, whereas the ionization yield of the spin-down photoelectron has the maximum at $\alpha = 90°$. For perpendicular alignment, the ionization yields of spin-up and spin-down photoelectrons are identical that leads to zero spin-polarization. Thus, except for $\alpha = 90°$ the nonadiabatic tunnel ionization of arbitrarily aligned NO (starting from the electronic ground state $|X\,^2\Pi_{1/2}\rangle$) by strong right circularly polarized laser pulses produces more spin-up photoelectrons than spin-down photoelectrons yielding non-zero and positive spin-polarization

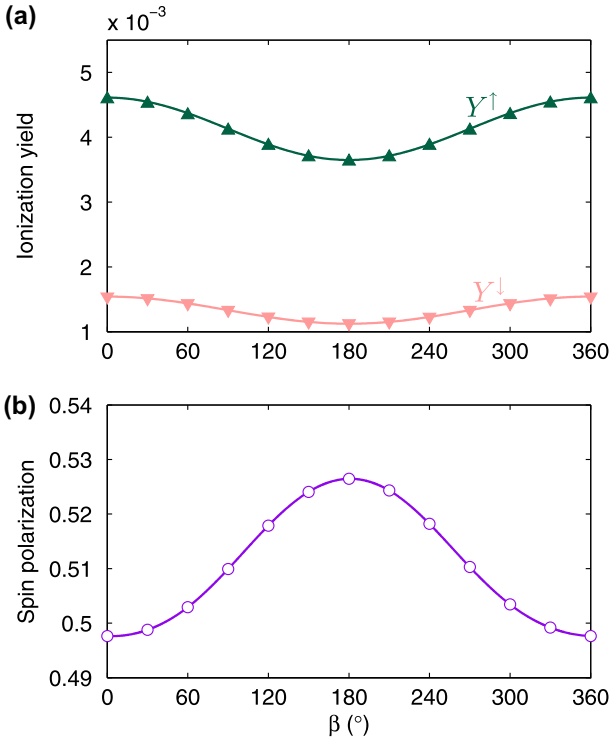

Figure 3. (a) Total ionization yields of spin-up $Y^{\uparrow}(\alpha, \beta)$ (green dark, Equation (29)) and spin-down $Y^{\downarrow}(\alpha, \beta)$ (red light, Equation (30)) photoelectrons and (b) spin polarization $\mathcal{P}(\alpha, \beta)$ (violet, Equation (32)) as functions of β for $\alpha = 10°$. The makers indicate the numerically calculated ionization yields (up- and down-pointed triangles) and spin polarization (circles), whereas the solid curves are the corresponding fitted curves. In particular, the fitted cosine curves in (a) are given by Equations (36) and (37).

of photoelectrons $\mathcal{P}(\alpha, \beta)$ (Equation (32)), see Figure 2(d). The spin polarization of the photoelectron is high for parallel alignment and decreases upon increasing the polar angle α to reach zero spin-polarization for perpendicular alignment. For ionization from the electronic state $|X\,^2\Pi_{3/2}\rangle$ of NO, strong right circularly polarized laser pulses then produce spin-down polarized photoelectrons, cf. Ref. (*27*). For ionization by strong left circularly polarized laser pulses, the corresponding spin-polarizations are reversed.

As already discussed above about the weak β-dependence, we present in Figure 3 our numerical results of the total ionization yields of spin-up $Y^{\uparrow}(\alpha, \beta)$ and spin-down $Y^{\downarrow}(\alpha, \beta)$ photoelectrons and spin polarization $\mathcal{P}(\alpha, \beta)$ as functions of the azimuthal angle β for the fixed polar angle $\alpha = 10°$. We have chosen $\alpha = 10°$ because the β-dependence of spin polarization for this polar angle is strongest, cf. Figure 2(d). In general, the ionization yields of photoelectrons are maximal for $\beta = 0°$ and minimal for $\beta = 180°$, whereas the spin polarization is minimal for $\beta = 0°$ and maximal for $\beta = 180°$. Again due to the heteronuclear character, we note that the results for $\beta = 90°$ and $\beta = 270°$

are not identical, therefore the ionization yields and spin poalarization are not exactly symmetrical. However, we draw the fitted cosine curves in Figure 3(a), where the markers in this figure indicate our numerical results. The relative deviations of the numerical results from the corresponding fitted curves for $\alpha = 10°$ are less than 0.13%. For other polar angles α, the maximal deviations are less than 2%. Therefore, the dependence of the ionization yields $Y^{\uparrow}(\alpha,\beta)$ and $Y^{\downarrow}(\alpha,\beta)$ on β can be approximately expressed as:

$$Y^{\uparrow}(\alpha,\beta) \approx \frac{1}{2}\left[Y^{\uparrow}(\alpha,0) + Y^{\uparrow}(\alpha,\pi)\right] + \frac{1}{2}\left[Y^{\uparrow}(\alpha,0) - Y^{\uparrow}(\alpha,\pi)\right]\cos\beta, \quad (36)$$

$$Y^{\downarrow}(\alpha,\beta) \approx \frac{1}{2}\left[Y^{\downarrow}(\alpha,0) + Y^{\uparrow}(\alpha,\pi)\right] + \frac{1}{2}\left[Y^{\downarrow}(\alpha,0) - Y^{\downarrow}(\alpha,\pi)\right]\cos\beta. \quad (37)$$

Then, using Equations (33) and (34), the average ionization yields of spin-up and spin-down photoelectrons from randomly aligned NO can be calculated as:

$$\overline{Y}^{\uparrow} \approx \frac{1}{4}\int_0^{\pi} \mathrm{d}\alpha \left[Y^{\uparrow}(\alpha,0) + Y^{\uparrow}(\alpha,\pi)\right]\sin\alpha, \quad (38)$$

$$\overline{Y}^{\downarrow} \approx \frac{1}{4}\int_0^{\pi} \mathrm{d}\alpha \left[Y^{\downarrow}(\alpha,0) + Y^{\downarrow}(\alpha,\pi)\right]\sin\alpha. \quad (39)$$

Finally, the average spin polarization of photoelectrons (Equation (35)) produced by nonadiabatic ionization of randomly aligned NO in strong three-cycle circularly polarized laser pulses with the laser wavelength $\lambda = 800$ nm and the laser intensity 1.76×10^{14} W/cm^2 is calculated as $\overline{\mathcal{P}} = 22.1\%$, see Figure 2(d). Of course, the average spin polarization for randomly aligned NO can be increased for larger values of Keldysh parameter, i.e. for shorter laser wavelengths and for lower laser intensities, cf. Ref. (*27*).

5. Conclusions

In the present paper, we have performed numerical calculations for tunnel ionization of NO for different molecular alignments in strong circularly polarized laser fields. With the fact that the electronic ground state $|X\,^2\Pi_{1/2}\rangle$ of NO possesses doubly degenerate $2\pi_-^{\uparrow}$ and $2\pi_+^{\downarrow}$ spin-orbitals with only one valence electron and the ionization of the counter-rotating orbital is preferred, cf. Ref. (*27*), strong circularly polarized laser fields can produce spin-polarized photoelectrons from NO. In particular, we have shown that in case of arbitrarily alinged NO, the counter-rotating orbital with respect to the circular polarization of the laser field projected on the plane perpendicular to the molecular axis is preferably ionized for all alignment angles except for perpendicular alignment. In this work, we have developed the theory of spin polarization of photoelectrons for arbitrary molecular alignment angles and predicted that strong circularly polarized laser fields can produce spin-polarized photoelectrons from randomly aligned NO.

Disclosure statement

No potential conflict of interest was reported by the authors.

Funding

This work was financially supported by the Max Planck Society via Max Planck Research Group 'Current-Carrying Quantum Dynamics' (CCQD); the Deutsche Forschungsgemeinschaft, Priority Programme 1840 'Quantum Dynamics in Tailored Laser Fields' (QUTIF).

References

(1) Krausz, F.; Ivanov, M. *Rev. Mod. Phys.* **2009,** *81,* 163–234.
(2) Ferray, M.; L'Huillier, A.; Li, X.F.; Lomprk, L.A.; Mainfray, G.; Manus, C. *J. Phys. B* **1988,** *21,* L31–L35.
(3) Corkum, P.B. *Phys. Rev. Lett.* **1993,** *71,* 1994–1997.
(4) Calegari, F.; Sansone, G.; Stagira, S.; Vozzi, C.; Nisoli, M. *J. Phys. B* **2016,** *49,* 062001.
(5) Marangos, J.P. *J. Phys. B* **2016,** *49,* 132001.
(6) Itatani, J.; Levesque, J.; Zeidler, D.; Niikura, H.; Pépin, H.; Kieffer, J.C.; Corkum, P.B.; Villeneuve, D.M. *Nature* **2004,** *432,* 867–871.
(7) Eckle, P.; Pfeiffer, A.N.; Cirelli, C.; Staudte, A.; Dörner, R.; Muller, H.G.; Büttiker, M.; Keller, U. *Science* **2008,** *322,* 1525–1529.
(8) Ivanov, I.A.; Kheifets, A.S. *Phys. Rev. A* **2014,** *89,* 021402(R).
(9) Morishita, T.; Le, A.-T.; Chen, Z.; Lin, C.D. *Phys. Rev. Lett.* **2008,** *100,* 013903.
(10) Meckel, M.; Comtois, D.; Zeidler, D.; Staudte, A.; Pavičić, D.; Bandulet, H.C.; Pépin, H.; Kieffer, J.C.; Dörner, R.; Villeneuve, D.M.; Corkum, P.B. *Science* **2008,** *320,* 1478–1482.
(11) Pullen, M.G.; Wolter, B.; Le, A.-T.; Baudisch, M.; Sclafani, M.; Pires, H.; Schröter, C.D.; Ullrich, J.; Moshammer, R.; Pfeifer, T.; Lin, C.D.; Biegert, J. *Nat. Commun.* **2016,** *7,* 11922.
(12) Xin, L.; Qin, H.; Wu, W.; He, F. *Phys. Rev. A* **2015,** *92,* 063803.
(13) Huismans, Y.; Rouzée, A.; Gijsbertsen, A.; Jungmann, J.H.; Smolkowska, A.S.; Logman, P.S.W.M.; Lépine, F.; Cauchy, C.; Zamith, S.; Marchenko, T.; Bakker, J.M.; Berden, G.; Redlich, B.; van der Meer, A.F.G.; Muller, H.G.; Vermin, W.; Schafer, K.J.; Spanner, M.; Ivanov, M.Y.; Smirnova, O.; Bauer, D.; Popruzhenko, S.V.; Vrakking, M.J.J. *Science* **2011,** *331,* 61–64.
(14) Zhou, Y.; Tolstikhin, O.I.; Morishita, T. *Phys. Rev. Lett.* **2016,** *116,* 173001.

(15) Madsen, C.B.; Anis, F.; Madsen, L.B.; Esry, B.D. *Phys. Rev. Lett.* **2012,** *109,* 163003.
(16) Liu, K.; Lan, P.; Huang, C.; Zhang, Q.; Lu, P. *Phys. Rev. A* **2014,** *89,* 053423.
(17) Zhang, W.; Li, Z.; Lu, P.; Gong, X.; Song, Q.; Ji, Q.; Lin, K.; Ma, J.; He, F.; Wu, J. *Phys. Rev. Lett.* **2016,** *117,* 103002.
(18) Milošević, D.B. *Phys. Rev. A* **2016,** *93,* 051402(R).
(19) Hartung, A.; Morales, F.; Kunitski, M.; Henrichs, K.; Laucke, A.; Richter, M.; Jahnke, T.; Kalinin, A.; Schöffler, M.; Schmidt, L.P.H.; Ivanov, M.; Smirnova, O.; Dörner, R. *Nat. Photon.* **2016,** *10,* 526–528.
(20) Barth, I.; Smirnova, O. *Phys. Rev. A* **2011,** *84,* 063415; **2012,** *85,* 029906(E); **2012,** *85,* 039903(E).
(21) Barth, I.; Smirnova, O. *Phys. Rev. A* **2013,** *87,* 013433.
(22) Barth, I.; Lein, M. *J. Phys. B* **2014,** *47,* 204016.
(23) Zhu, X.; Lan, P.; Liu, K.; Li, Y.; Liu, X.; Zhang, Q.; Barth, I.; Lu, P. *Opt. Express* **2016,** *24,* 4196–4209.
(24) Herath, T.; Yan, L.; Lee, S.K.; Li, W. *Phys. Rev. Lett.* **2012,** *109,* 043004.
(25) Barth, I.; Smirnova, O. *Phys. Rev. A* **2013,** *87,* 065401.
(26) Barth, I.; Smirnova, O. *Phys. Rev. A* **2013,** *88,* 013401.
(27) Liu, K.; Barth, I. *Phys. Rev. A* **2016,** *94,* 043402.
(28) Walser, M.W.; Keitel, C.H. *Opt. Commun.* **2001,** *199,* 447–451.
(29) Faisal, F.H.M.; Bhattacharyya, S. *Phys. Rev. Lett.* **2004,** *93,* 053002.
(30) Barth, I.; Manz, J.; Serrano-Andrés, L. *Chem. Phys.* **2008,** *347,* 263–271.
(31) Barth, I.; Serrano-Andrés, L.; Seideman, T. *J. Chem. Phys.* **2008,** *129,* 164303; **2009,** *130,* 109901.
(32) Endo, T.; Matsuda, A.; Fushitani, M.; Yasuike, T.; Tolstikhin, O.I.; Morishita, T.; Hishikawa, A. *Phys. Rev. Lett.* **2016,** *116,* 163002.
(33) Pavičić, D.; Lee, K.F.; Rayner, D.M.; Corkum, P.B.; Villeneuve, D.M. *Phys. Rev. Lett.* **2007,** *98,* 243001.
(34) Petretti, S.; Vanne, Y.V.; Saenz, A. *Phys. Rev. Lett.* **2010,** *104,* 223001.